

Novel Tools and Methods

A Cre Driver Line for Genetic Targeting of Kappa Opioid Receptor Expressing Cells

Franciely Paliarin,^{1,*} Chelsea Duplantis,^{1,*} Andrea F. Jones,¹ Jessica Cucinello-Ragland,¹ Samhita Basavanhalli,¹ Emily Blaze,¹ Evan Doré,¹ Anna Isabella Neel,² Haiguo Sun,²  Rong Chen,² Scott Edwards,¹  Nicholas W. Gilpin,¹  Robert O. Messing,³ and Rajani Maiya¹

<https://doi.org/10.1523/ENEURO.0043-23.2023>

¹Department of Physiology, LSU Health Sciences Center, New Orleans, Louisiana 70112, ²Department of Physiology and Pharmacology, Wake Forest University School of Medicine, Winston-Salem, North Carolina 27157, and ³Department of Neuroscience and Waggoner Center for Alcohol and Addiction Research, The University of Texas at Austin, Austin, Texas 78712

Abstract

Here we describe the generation and characterization of a *Cre* knock-in mouse line that harbors a *Cre* insertion in the 3'UTR of the κ opioid receptor gene (*Oprk1*) locus and provides genetic access to populations of κ opioid receptor (KOR)-expressing neurons throughout the brain. Using a combination of techniques including RNA *in situ* hybridization and immunohistochemistry, we report that *Cre* is expressed with high fidelity in KOR-expressing cells throughout the brain in this mouse line. We also provide evidence that *Cre* insertion does not alter basal KOR function. Baseline anxiety-like behaviors and nociceptive thresholds are unaltered in *Oprk1-Cre* mice. Chemogenetic activation of KOR-expressing cells in the basolateral amygdala (BLA^{KOR} cells) resulted in several sex-specific effects on anxiety-like and aversive behaviors. Activation led to decreased anxiety-like behavior on the elevated plus maze and increased sociability in female but not in male *Oprk1-Cre* mice. Activation of BLA^{KOR} cells also attenuated KOR agonist-induced conditioned place aversion (CPA) in male *Oprk1-Cre* mice. Overall, these results suggest a potential role for BLA^{KOR} cells in regulating anxiety-like behaviors and KOR-agonist mediated CPA. In summary, these results provide evidence for the utility of the newly generated *Oprk1-Cre* mice in assessing localization, anatomy, and function of KOR circuits throughout the brain.

Key words: anxiety; conditioned place aversion; dynorphin; genetic access; knock-in mice; social interaction

Significance Statement

Here we report the generation and characterization of an *Oprk1-Cre* mouse line that harbors *Cre* insertion in the 3'UTR of the *Oprk1* locus. There is high fidelity of *Cre* expression to KOR-expressing cells throughout the brain in this mouse line and *Cre* insertion does not impair KOR function. Chemogenetic activation of BLA^{KORs} led to sex-specific effects on anxiety-like behaviors and attenuated KOR agonist-induced conditioned place aversion. These results provide evidence for the utility of the newly generated *Oprk1-Cre* mice to interrogate KOR function in discreet circuits.

Introduction

The κ opioid receptor (KOR) is a member of the opioid receptor family that is widely expressed throughout the CNS and peripheral nervous system. The KORs belong to

the seven-transmembrane G-protein-coupled receptor superfamily and are coupled to $G\alpha_{i/o}$ proteins. Dynorphin

Received February 5, 2023; accepted June 16, 2023; First published June 26, 2023.

The authors declare no competing financial interests.

Author contributions: F.P., C.D., A.F.J., R.C., N.W.G., R.O.M., and R.M. designed research; F.P., C.D., A.F.J., J.C.-R., S.B., E.B., E.D., A.I.N., H.S., and R.C. performed research; F.P., C.D., A.F.J., J.C.-R., S.B., E.B., E.D., H.S., R.C., S.E., and R.M. analyzed data; F.P., A.F.J., J.C.-R., R.C., S.E., N.W.G., R.O.M., and R.M. wrote the paper.

(Dyn) is the primary endogenous ligand for KORs. Upon agonist binding to KORs, activated $G_{\alpha_{i/o}}$ subunits inhibit adenylyl cyclase and therefore decreased cAMP production. The released $G_{\beta\gamma}$ subunits block Ca^{+2} channels and activate GIRK channels (Al-Hasani and Bruchas, 2011; Crowley and Kash, 2015). The net result of these events is hyperpolarization of the cell and therefore decreased likelihood of action potential firing. In addition, agonist binding at KORs activates other intracellular signaling cascades including the extracellular signal-regulated kinase (ERK) 1/2, p38 MAPK, and JNK pathways (Bruchas et al., 2006, 2007a, b). A large body of preclinical literature implicates a role for the Dyn/KOR system in regulating mood, reward-related processes, pain, and cognition (Bruchas et al., 2010; Al-Hasani and Bruchas, 2011; Crowley and Kash, 2015; Abraham et al., 2021). Activation of the KORs *in vivo* results in dysphoric and anhedonic states and induces conditioned place avoidance (CPA) in rodents (Bruchas et al., 2010; Al-Hasani and Bruchas, 2011; Crowley and Kash, 2015; Abraham et al., 2021). However, insight into the role of KORs in these behaviors was primarily derived from pharmacological and genetic manipulation studies leaving open questions regarding the precise cellular and circuit location of KORs mediating these behavioral effects.

KORs and their endogenous ligand Dyn are widely expressed in the adult brain, including basolateral amygdala (BLA) nucleus and central nucleus of the amygdala (CeA), the nucleus accumbens (NAc), caudate, putamen, paraventricular thalamus (PVT), hypothalamus, and ventral tegmental area (VTA; DePaoli et al., 1994). The Dyn/KOR system is heavily implicated in mediating the behavioral effects of stress (Bruchas et al., 2010; Crowley and Kash, 2015). Stressful events can cause the release of Dyn in a variety of brain regions, and Dyn-mediated activation of KORs is thought to contribute to dysphoria and negative affective states that result from chronic stress (Bruchas et al., 2010; Crowley and Kash, 2015). Moreover, there is also strong evidence that KORs play a role in substance use disorders (Nestler, 1996). Specifically, the Dyn/KOR system is thought to contribute to the negative affective and dysphoric state referred to as “the dark side” of addiction that results from chronic drug use and leads to further escalation of drug intake (Chavkin and Koob, 2016). Stress is a risk factor for major depressive disorders (Nemeroff and Vale, 2005) and KOR antagonists are currently being investigated for therapeutic efficacy in the

treatment of depression (Krystal et al., 2020). Further, KORs are also expressed in nociceptor populations in the periphery as well as in brain regions involved in pain. KOR agonists have marked analgesic properties and are also being investigated as a therapeutic target for acute and chronic pain (Snyder et al., 2018). KOR agonists are also antipruritic and inhibit itching caused by a variety of pruritogens (Nguyen et al., 2021; Inan and Cowan, 2022). Hence, KORs have emerged as promising therapeutic candidates for the treatment of a wide range of neuropsychiatric disorders ranging from depression and addiction to pain and pruritis.

Despite tremendous interest in therapeutics targeting KORs, the cellular and circuit mechanisms by which KORs mediate these diverse behaviors remain largely unknown. Tools to manipulate KOR-expressing cells in the brain and periphery were lacking until recently. A recently generated *Oprk1-Cre* mouse harbors Cre insertion in the second exon of the *Oprk1* locus that may disrupt endogenous gene transcription (Cai et al., 2016). In this article, we describe the generation and characterization of a novel *Oprk1-Cre* mouse that harbors a Cre insertion in the 3'UTR of the *Oprk1* locus. We verify the fidelity of Cre expression in this mouse line using a variety of methods. We also show that Cre insertion into the *Oprk1* locus does not alter KOR function or baseline anxiety-like and pain-like behaviors. We also show that the activation of BLA^{KORs} is anxiolytic in females and attenuates KOR agonist-induced CPA in males.

Materials and Methods

Mice

Oprk1-Cre mice harboring a Cre insertion in the 3'UTR of the *Oprk1* locus were generated by Cyagen using homologous recombination. Briefly, the TGA stop codon at the *Oprk1* locus was replaced by a “P2A-Cre” cassette (Extended Data Fig. 1-1). The targeting vector contained homology arms that were generated using the BAC (bacterial artificial chromosome) clone as a template. The Neo cassette in the targeting vector was flanked by self-deletion anchor sites. C57BL/6N embryonic stem (ES) cells were used for gene targeting. A targeted ES cell clone harboring the correct insertion was injected into C57BL/6N embryos before being implanted into a pseudopregnant CD1 female. Founder animals were identified by coat color, and their germline transmission was confirmed by breeding with C57BL/6N females and subsequent genotyping of the offspring. Mice were genotyped by Transnetyx. All mice were provided access to food and water *ad libitum* and housed in reverse light/dark cycle (on at 10:00 A.M., off 10:00 P.M.). Animals that went surgical procedures were singly housed postsurgery before behavioral analyses. *Oprk1-Cre* mice that were backcrossed to C57BL/6J mice for at least three generations were used in this study. Only heterozygous *Oprk1-Cre* mice and their wild-type (WT) littermates were used for all behavioral, Western blotting, immunohistochemistry (IHC), [³⁵S] GTP- γ S, and quantitative PCR (qPCR) experiments. Homozygous Cre mice were used for *in situ* hybridization to verify the fidelity of Cre and *Oprk1* expression. For behavioral experiments, male and female mice were tested concurrently in mixed sex cohorts. Floxed L10A-

This work was supported in part by National Institute on Alcohol Abuse and Alcoholism Grant AA-027293 (R.M.).

Acknowledgments: We thank Matthew Brian Pomrenze and Mike Salling for many helpful discussions. We also thank Emily Garcia for help with RNA *in situ* hybridizations. In addition, we thank Christoph Kellendonk for the gift of the Cre antibody.

*F.P. and C.D. contributed equally to this work.

Correspondence should be addressed to Rajani Maiya at rmaiya@lsuhsc.edu.

<https://doi.org/10.1523/ENEURO.0043-23.2023>

Copyright © 2023 Paliarin et al.

This is an open-access article distributed under the terms of the Creative Commons Attribution 4.0 International license, which permits unrestricted use, distribution and reproduction in any medium provided that the original work is properly attributed.

EGFP mice were obtained from Bradford Lowell (Harvard University, Boston, MA) and have been previously described (Krashes et al., 2014).

Drugs and viral vectors

U-50488 (Tocris Bioscience) was dissolved in saline and injected intraperitoneally at 10 mg/kg for biochemistry experiments and 2.5 mg/kg for CPA experiments (10 ml/kg). Clozapine *N*-oxide (CNO; free base) was obtained from Hello Bio and dissolved in saline containing 0.5% DMSO. Mice were injected with 3–5 mg/kg CNO (at 10 ml/kg) 30 min before behavioral testing. The Cre-dependent viral vectors AAV8-hSyn-DIO-hM3DQ-mCherry, AAV8-hSyn-DIO-mCherry, AAV8-hSyn-DIO-EGFP were obtained from Addgene. The titers of all AAVs were $\sim 3\text{--}5 \times 10^{12}$ infectious units/ml.

Stereotaxic surgeries

Adeno-associated virus (AAV; 100 nl) encoding either Cre-dependent mCherry or hM3DQ, as described previously (Lasek and Azouaou, 2010; Maiya et al., 2021), were infused bilaterally into the BLA of male and female *Oprk1-Cre* mice using an injector (Nanoject III, Drummond Scientific). The coordinates for BLA were as follows: anteroposterior, -1.6 mm from skull; mediolateral, ± 3.25 mm from skull; dorsoventral, -4.5 mm from skull. Mice were allowed to recover for 2 weeks before behavioral testing.

Immunohistochemistry for Cre recombinase

Mice were perfused transcardially with PBS followed by 4% paraformaldehyde (PFA) in PBS, pH 7.4. Brains were extracted, postfixed overnight in the same fixative, and cryoprotected in 30% sucrose in PBS at 4°C. Brains were sectioned at 40 μ m thickness on a cryostat, and free-floating sections were collected in PBS. Sections were washed three times in PBS containing 0.2% Triton X-100 (PBST) for 10 min at 27°C, incubated in 3% hydrogen peroxide for 5 min, and washed 3×10 min in PBS. Sections were then blocked for 1 h in PBS containing 0.3% Triton X-100 and 1% BSA at 27°C, and incubated in 1:700 dilution of rabbit anti-Cre antibody (gift from C. Kellendonk, Columbia University, New York, NY) for 24 h at 4°C on a rocker. Sections were then washed $1 \times$ in 0.1 M Tris-Cl, pH 7.4, 150 mM NaCl, and 0.3% Triton X-100 (TNT buffer) for 10 min followed by incubation in 0.1 M Tris-Cl, pH 7.4, 150 mM NaCl, and 0.5% TSA blocking reagent (TNB buffer; Akoya Biosciences) for 30 min. This was followed by incubation in ImmPRESS HRP Horse Anti-Rabbit HRP-conjugated secondary antibody (Vector Laboratories) for 1 h. Sections were then washed $4 \times$ for 5 min in TNT buffer followed by incubation in trichostatin A (TSA) reagent (fluorescein in 1:50 TSA amplification diluent; Akoya Biosciences). Following this incubation, sections were washed $3 \times$ for 10 min in TNT buffer, mounted on slides and coverslipped with Fluormount G (Southern Biotech) mounting media containing DAPI. Tiled images of the entire brain were acquired at 20 \times resolution on a microscope (model BX51, Olympus).

RNA *in situ* hybridization

We performed fluorescence *in situ* hybridization to examine colocalization between *Oprk1* and *Cre* transcripts.

Mouse brains were rapidly extracted by decapitation and flash frozen in a dry ice/isopentane bath. Coronal sections (12 μ m) were obtained and mounted on a glass slide. *In situ* hybridization was performed using RNAScope Fluorescent Multiplex Kit (Advanced Cell Diagnostics). The following probes were used for RNAScope: *Oprk1* (catalog #31611); *Cre* (catalog #423321); and EGFP-04 (catalog #538851). Slides were coverslipped with Fluormount-G with DAPI (Southern Biotech) and imaged using a confocal microscope (Leica) at 20 \times resolution. The extent of colocalization between *Oprk1* and *Cre* was determined using Fiji as previously described (Schindelin et al., 2012; Pomrenze et al., 2019; Maiya et al., 2021). To determine colocalization between virally expressed Cre-dependent EGFP and *Oprk1*, mice were killed 2 weeks postsurgery.

Validation of designer receptors activated by designer drug-induced activation of BLA^{KOR} neurons

Oprk1-Cre mice expressing hM3DQ in the BLA were administered either vehicle or CNO (3 mg/kg) 90 min before being killed. Mice were perfused transcardially with PFA, and the brain was removed, postfixed, and processed for IHC, as described in subsection Immunohistochemistry for Cre recombinase. Sections were incubated with Rabbit c-Fos antibody (catalog #226-003, Synaptic Systems) at 1:1000 dilution with a 1:5000 dilution of mouse anti-mCherry antibody (catalog #632453, Clontech) overnight at 4°C. Alexa Fluor-conjugated secondary antibodies were used to detect primary antibody binding as described above. c-Fos as a marker for neural activity was quantified using a custom macro in FIJI (Schindelin et al., 2012).

RNA extractions and quantitative PCR

Brains were extracted from male and female WT and heterozygous *Oprk1-Cre* mice (age range, $\sim 8\text{--}12$ weeks) and flash frozen. Brains were homogenized using a Dounce homogenizer, and total RNA was isolated using the RNAEasy Midi Kit (Qiagen) following manufacturer instructions. RNA was treated with DNase (Ambion). Total RNA was quantified on a NanoDrop 1000 Spectrophotometer (Thermo Fisher Scientific). RNA (1 mg) was reverse transcribed using the High-Capacity Reverse Transcription Kit from Applied Biosystems. cDNA was diluted 1:5, and 2 μ l of that solution were subjected to real-time PCR amplification to detect *Oprk1* (Mm01230885_m1, Thermo Fisher Scientific) with 5 μ l of 1 \times SSoAdvanced Universal Probes Master Mix (BIO-RAD), 0.5 μ l of 20 \times TaqMan Primer/Probe Mix (Applied Biosystems) in a total volume of 10 μ l. Data were normalized to the endogenous control genes for transferrin (*Tfrc*; Mm00441941_m1, Thermo Fisher Scientific) or gusducin B (*Gusb*; Mm019768_m1, Thermo Fisher Scientific).

Western blotting

Heterozygous *Oprk1-Cre* and their WT littermates were killed by cervical decapitation, and their brains were rapidly removed and frozen in isopentane. Brains were sectioned at 300 μ m thickness on the cryostat, and the amygdala (AMY, BLA+CeA) and NAc were dissected using a 2 mm biopsy punch. Tissue samples were homogenized in lysis

buffer containing 320 mM sucrose, 5 mM HEPES, 1 mM EGTA, 1 mM EDTA, and 1% SDS, protease inhibitor cocktail (diluted 1:100), and phosphatase inhibitor cocktails II and III (diluted 1:100; Sigma-Aldrich) followed by brief sonication and then heating at 95°C for 5 min. Protein concentration was determined by a colorimetric Lowry assay (DC protein assay, BIO-RAD). Protein (20 µg) was resolved on a 10% SDS-polyacrylamide gel and electrophoretically transferred onto a polyvinylidene difluoride membrane. After the transfer, membranes were blocked with 5% nonfat dry milk (NFDM) in tris-buffered saline containing Tween-20 (TTBS) for 1 h at room temperature followed by overnight incubation at 4°C with primary antibody in 5% NFDM in TTBS, as shown in Extended Data Table 3-1. Membranes were washed in TTBS 3× for 10 min at 27°C, labeled with appropriate peroxidase-conjugated secondary antibodies (1:10,000 in TTBS; BIO-RAD), washed again 3× in TTBS, incubated in chemiluminescent reagent (Immobilon Crescendo Western HRP substrate, Millipore Sigma), and exposed to film. Membranes were stripped and reprobed using a primary antibody in 2.5% milk in TTBS for total protein levels for each protein target in Extended Data Table 3-1. Densitometric analyses was performed using FIJI. Phosphoprotein levels were normalized to total protein levels, and results were expressed as a percentage of the mean of the WT values for each gel to normalize data across blots.

Striatal membrane preparation and [³⁵S]GTP γ S binding

Mouse striatum, including both ventral and dorsal striatum, were dissected from adult mice and frozen at -80°C. To prepare membranes, striatal tissue was homogenized using a Dounce homogenizer in cold homogenization buffer containing 10 mM Tris-HCl, pH 7.4, 100 mM NaCl, and 1 mM EDTA, as described previously (Bohn et al., 2015; Zhou et al., 2015). Homogenates were centrifuged at 20,000 × *g* for 30 min at 4°C. The resulting pellet was resuspended in homogenization buffer and incubated at 37°C for 30 min to remove endogenous opioids (McDonald and Lambert, 2010). The homogenate was centrifuged again at 20,000 × *g* for 30 min at 4°C, followed by resuspension in homogenization buffer and centrifugation. The resulting pellet was then resuspended in the assay buffer (10 mM Tris-HCl, pH 7.4, 100 mM NaCl, 1 mM EDTA, 5 mM MgCl₂). Membrane protein concentration was determined using the BCA Protein Assay (catalog #23225, Thermo Fisher Scientific), followed by addition of 1 mM DTT (final concentration) to the membranes. Membranes were stored at -80°C for future analysis.

For [³⁵S] GTP γ S binding, striatal membrane proteins (2.5 µg) were incubated in the assay buffer containing 1 nM [³⁵S] GTP γ S, 10 µM GDP, and increasing concentrations of Dyn A (10 nM to 10 µM) for 1 h at 30°C in a total volume of 100 µl. The reactions were terminated by transferring reaction mixture onto GF/B filters using a 96-well plate harvester followed by three washes with ice-cold assay buffer. The membrane-bound [³⁵S]GTP γ S was retained on the filters, whereas free [³⁵S]GTP γ S was washed off. Filters were dried for a couple hours, and radioactivity was determined with a TopCount Microplate Scintillation

Counter (PerkinElmer). Nonspecific binding was determined in the presence of 10 µM GTP γ S, and the basal binding was determined in the absence of Dyn. Specific GTP γ S binding was calculated by subtracting nonspecific activity from the total binding. Data were presented as a fold change over the basal activity. The sigmoidal Dyn dose-response curves were generated using the three-parameter nonlinear regression analysis. The values for EC₅₀ and maximal stimulation (E_{max}) were extrapolated from the curves.

Elevated plus maze

The elevated plus maze (EPM) consisted of two open and two closed arms perpendicular to each other. The maze was elevated ~40 cm above the ground. The open arms measured 40 cm long × 5 cm wide. The closed arms were identical to the open arms but were enclosed by a 19-cm-high wall. The session was performed under dim white light. Mice were placed in the center of the maze facing the open arms and allowed to explore the maze for 5 min. The entire session was recorded using a video camera, and the results were scored manually by an observer blind to the genotype and experimental conditions. Parameters measured included the percentage of open arm entries as well as the percentage of time spent in open arms. For experiments examining the consequences of chemogenetic activation of BLA^{KOR} cells, all mice (mCherry-injected and hM3DQ-injected mice) were injected with the designer receptors exclusively activated by designer drug (DREADD) agonist CNO (3 mg/kg) 30 min before being placed on the elevated plus maze. Mice were tested using the same parameters used for baseline behavioral testing.

Open field test

Mice were placed in a 43 × 43 cm open field chamber under dim white light for 10 min. The entire session was recorded using a video camera, and the results were analyzed using Biobserve Viewer III to determine the amount of time spent in the center and the periphery of the open field. *Oprk1-Cre* mice injected in the BLA with AAVs encoding either hM3DQ or mCherry were administered CNO (3 mg/kg, i.p.) 30 min before being placed in the open field chamber.

Electronic von Frey

An electronic von Frey (eVF) apparatus (TopCat Metrology) was used to measure mechanical nociception. Mice were acclimated in elevated acrylic compartments (11 × 14 × 21.5 cm) on a mesh stand for at least 5 min before testing. Following this acclimation period, an eVF filament was applied to the mid-plantar region of the hind-paw, and withdrawal thresholds were recorded. The filament was applied to alternating left and right hind-paws at 3 min intervals for a total of two measurements per paw. The average score of these four tests served as the dependent measure.

Thermal nociception tests

Thermal nociception was evaluated with a hot plate or cold plate apparatus, with a 20 × 20 cm metal surface

maintained at either 54°C or 3°C and surrounded by a 26-cm-high Plexiglas wall. The nociceptive response was defined as the paw withdrawal latency in seconds. A sharp withdrawal, licking, or shaking of any hindpaw was considered a positive response.

U-50488-induced conditioned place aversion and CNO conditioning

Mice were trained in a 27.3 × 27.3 cm² open-field apparatus (Med Associates) equipped with two chambers that had different floor textures (rods and holes) and wall patterns (vertical and horizontal stripes). The two chambers were separated by a Plexiglas door that was open during the habituation and test sessions and closed during training sessions. Before training, drug-naïve hM3DQ and control mCherry-injected mice were habituated to the apparatus and allowed access to both chambers for 15 min in a pretest session. Mice were administered 5 mg/kg (i.p.) CNO 30 min before the conditioning session followed by 2.5 mg/kg (i.p.) U-50488 15 min before the session. The study design was unbiased in that half of the mice received the drug in their preferred compartment, whereas half of them received the drug in their nonpreferred compartment. For CPA experiments, mice received two conditioning sessions per day. The first conditioning session was in the morning when mice received vehicle injections and were confined to one side of the chamber for 30 min. In the afternoon session, mice were injected with U-50488 and CNO and were confined to the other side of the chamber for 30 min. They received three vehicle and three CNO/U-50488 pairings. Twenty-four hours after the last conditioning session, mice were allowed access to both chambers for 15 min. A difference score was defined as the difference in the percentage of time spent in the drug (U-50488/CNO)-paired compartment postconditioning minus the time spent in the drug-paired compartment preconditioning. For experiments in WT mice, there were two groups. One group received saline on both sides of the compartment and another group received saline on one side and U-50488 (2.5 mg/kg) on the other side. Pretest, conditioning, and post-test sessions were conducted as described above.

We also examined whether activation of BLA^{KOR} cells was inherently rewarding or aversive using a place-conditioning test. CNO conditioning was done exactly as outlined above using an unbiased design. Mice received CNO (5 mg/kg, i.p.) and were confined to one side of the chamber for 30 min. The next day they received an equal volume of vehicle (10 ml/kg) and were confined to the opposite side. Mice were subjected to one conditioning session per day. They received four vehicle and four CNO pairings. Twenty-four hours after the last conditioning session, all mice were allowed access to both chambers for 15 min in a post-test session. A difference score was calculated as above.

Three-chambered social interaction test

The three-chambered social interaction was performed in a Plexiglas box [60 (length) × 40 (width) × 22 (height)

cm] composed of three chambers. Two empty inverted wire cups were placed in the outer chambers of the apparatus, and mice were acclimated to the apparatus for 5 min, 24 h before the start of the test. On the day of the test, mice were injected with CNO (5 mg/kg, i.p.), 30 min before the start of the test. An age-matched and sex-matched unfamiliar conspecific (target mouse) was placed under one of the wire cups. The wire cup in the other outer chamber was left empty. The side of the chamber that had the target mouse was alternated between the two outer chambers. A mouse was placed in the box for 10 min, and the amount of time that the mouse spent in each of the chambers was recorded. The entire session was recorded using a video camera, and time spent in each chamber was scored using Biobserve Viewer III. A sociability index was calculated for each mouse as (time spent in chamber with target mouse – time spent in chamber with empty cup)/(time spent in chamber with target mouse + time spent in chamber with empty cup).

Electrophysiology

Mice were briefly (~15–20 s) anesthetized with isoflurane, brains were rapidly removed, and placed in ice-cold choline buffer [(in mM) 25 NaHCO₃, 1.25 NaH₂PO₄, 2.5 KCl, 0.5 CaCl₂, 7 MgCl₂, 25 D-glucose, 110 C₅H₁₄GINO (choline chloride), 11.60 C₆H₇NaO₆ (sodium ascorbate), and 3.09 C₃H₃NaO₃ (sodium pyruvate)] for sectioning. Coronal slices, 300 μm thick, containing BLA were prepared using a VT1200s Leica Vibratome and transferred to artificial CSF (ACSF; 127 mM NaCl, 25 mM NaHCO₃, 1.25 mM NaH₂PO₄, 2.5 mM KCl, 25 mM D-glucose, 2 mM CaCl₂, 1 mM MgCl₂) in a water bath for 30 min at 37°C. Slices then remained at room temperature until they were used for recordings. ACSF was continually perfused over the slice during recordings at a rate of ~2 ml/min and maintained at ~32–34°C, and slices were continuously aerated with a 5% carbon/95% oxygen mixture throughout preparation and recording. Slices and ACSF were replaced either after each recording or every hour between recordings to ensure optimal recording conditions.

Borosilicate glass pipettes (World Precision Instruments) with series resistances between 3 and 6 MΩ were fabricated using a horizontal puller (model P-97, Sutter Instruments). Pipette capacitance was compensated but series resistance was not. A potassium-based internal solution was used for all recordings (128 mM K-gluconate, 10 mM HEPES, 10 mM sodium phosphocreatine, 4 mM magnesium chloride, 4 mM sodium ATP, 0.4 mM sodium GTP, 3 mM ascorbic acid, 1 mM EGTA, and in some cases ~3.5 mg/ml biocytin). Blockers were not used for any of the recordings. hM3DQ-labeled cells were visualized using an inverted microscope with 10× and 60× objectives (Olympus) coupled with a Prizmatix LED system (Prizmatix LTD). Series resistance for each neuron was recorded in voltage-clamp mode and was required to be <30 MΩ for inclusion in the analysis. Neuronal properties were recorded in current-clamp mode at resting membrane potential and at holding potential (by injecting additional current to maintain the cell at –70 mV). Frequency/current responses (duration, 1 s; amplitude, –200 to 200 pA; 20 pA steps) and spontaneous

Table 1: Table of summary statistics

Figure	Parameter	Type of test	Sample size	Statistical data
3A	[³⁵ S]GTP γ S binding	Nonlinear curve fit	WT male = 7 <i>Cre</i> /+ male = 7	EC_{50} WT = 1.33×10^{-7} M for WT and 1.268×10^{-7} for <i>Cre</i> /+ $R_2 = 0.7756$ for WT and 0.7597 for <i>Cre</i> /+
3B	P-ERK levels normalized to T-ERK	Unpaired <i>t</i> test Two tailed	WT female = 4, <i>Cre</i> /+ female = 3, <i>Cre</i> /+ male = 2	$t = 0.68$, $df = 10$, $p = 0.51$
3C	P-JNK levels to T-JNK	Unpaired <i>t</i> test, two-tailed	WT female = 4, <i>Cre</i> /+ female = 3, <i>Cre</i> /+ male = 2	$t = 0.498$, $df = 7$, $p = 0.6335$
3D	P-p38 levels normalized to total p38	Unpaired <i>t</i> test, two-tailed	WT female = 4, <i>Cre</i> /+ female = 3, <i>Cre</i> /+ male = 2	$t = 0.043$, $df = 10$. $p = 0.97$
4A	Elevated plus maze, percentage open arm entries	Two-way ANOVA	WT male = 7, WT female = 12; <i>Cre</i> /+ male = 8, <i>Cre</i> /+ female = 7	$F_{\text{genotype}}(1,30) = 0.21$, $p = 0.66$ $F_{\text{sex}}(1,30) = 4.2$, $p = 0.049$ $F_{\text{genotype} \times \text{sex}}(1,30) = 0.32$, $p = 0.57$
4B	Elevated plus maze, percentage open arm time	Two-way ANOVA	WT male = 7, WT female = 12; <i>Cre</i> /+ male = 8, <i>Cre</i> /+ female = 7	$F_{\text{genotype}}(1,30) = 0.74$, $p = 0.4$ $F_{\text{sex}}(1,30) = 0.99$, $p = 0.33$ $F_{\text{genotype} \times \text{sex}}(1,30) = 0.46$, $p = 0.50$
4C	Percentage time in center, open field	Two-way ANOVA	WT male = 8, WT female = 11; <i>Cre</i> /+ male = 9, <i>Cre</i> /+ female = 7	$F_{\text{genotype}}(1,31) = 1.97$, $p = 0.17$ $F_{\text{sex}}(1,31) = 4.4$, $p = 0.04$ $F_{\text{genotype} \times \text{sex}}(1,31) = 0.00003$, $p = 0.99$
4D	Mean withdrawal threshold, electronic von Frey	Two-way ANOVA	WT male = 8, WT female = 10; <i>Cre</i> /+ male = 8, <i>Cre</i> /+ female = 7	$F_{\text{genotype}}(1,29) = 0.18$, $p = 0.68$ $F_{\text{sex}}(1,29) = 9.82$, $p = 0.0039$ $F_{\text{genotype} \times \text{sex}}(1,29) = 3.78$, $p = 0.06$
4E	Response latency, hot plate	Two-way ANOVA	WT male = 8, WT female = 10; <i>Cre</i> /+ male = 8, <i>Cre</i> /+ female = 7	$F_{\text{genotype}}(1,29) = 1.28$, $p = 0.27$ $F_{\text{sex}}(1,29) = 3.76$, $p = 0.06$ $F_{\text{genotype} \times \text{sex}}(1,29) = 2.58$, $p = 0.12$
4F	Response latency, cold plate	Two-way ANOVA	WT male = 8, WT female = 9; <i>Cre</i> /+ male = 9, <i>Cre</i> /+ female = 7	$F_{\text{genotype}}(1,29) = 0.09$, $p = 0.77$ $F_{\text{sex}}(1,29) = 1.7$, $p = 0.2$ $F_{\text{genotype} \times \text{sex}}(1,29) = 1.94$, $p = 0.17$
5B	Number of action potentials	Paired <i>t</i> test, two-tailed	Baseline = 7, CNO = 7	$t = 3.08$, $df = 9$, $p = 0.022$
5C	Resting membrane potential	Paired <i>t</i> test, two-tailed	Baseline = 7, CNO = 7	$t = 3.757$, $df = 9$, $p = 0.0094$
5E	c-Fos counts	Unpaired <i>t</i> test, two-tailed	Veh = 3, CNO = 4	$t = 4.995$, $df = 5$, $p = 0.0041$
7A	Elevated plus maze, percentage open arm entries	Two-way ANOVA	mCherry male = 8, mCherry female = 10; hM3DQ male = 8, hM3DQ female = 9	$F_{\text{virus}}(1,31) = 6.64$, $p = 0.015$ $F_{\text{sex}}(1,31) = 2.51$, $p = 0.12$ $F_{\text{virus} \times \text{sex}}(1,31) = 7.49$, $p = 0.01$
7B	Elevated plus maze, percentage open arm time	Two-way ANOVA	mCherry male = 8, mCherry female = 10; hM3DQ male = 8, hM3DQ female = 9	$F_{\text{virus}}(1,31) = 9.4$, $p = 0.005$ $F_{\text{sex}}(1,31) = 5.07$, $p = 0.032$ $F_{\text{virus} \times \text{sex}}(1,31) = 12.22$, $p = 0.001$
7C	Percentage time in center, open field	Two-way ANOVA	mCherry male = 9, mCherry female = 11; hM3DQ male = 9, hM3DQ female = 9	$F_{\text{virus}}(1,34) = 1.12$, $p = 0.29$ $F_{\text{sex}}(1,34) = 0.03$, $p = 0.87$ $F_{\text{virus} \times \text{sex}}(1,34) = 0.48$, $p = 0.49$
7D	Sociability index	Two-way ANOVA	mCherry male = 9, mCherry female = 11; hM3DQ male = 9, hM3DQ female = 10	$F_{\text{virus}}(1,35) = 0.48$, $p = 0.83$ $F_{\text{sex}}(1,35) = 0.01$, $p = 0.92$ $F_{\text{virus} \times \text{sex}}(1,35) = 6.76$, $p = 0.01$
8A	U-50488 CPA, difference score	Two-way ANOVA	mCherry male = 9, mCherry female = 10; hM3DQ male = 8, hM3DQ female = 11	$F_{\text{virus}}(1,34) = 1.656$, $p = 0.21$ $F_{\text{sex}}(1,34) = 0.016$, $p = 0.89$ $F_{\text{virus} \times \text{sex}}(1,34) = 4.67$, $p = 0.037$

(Continued)

Table 1: Continued

Figure	Parameter	Type of test	Sample size	Statistical data
8B	CNO CPP, difference score	Two-way ANOVA	mCherry male = 5, mCherry female = 7; hM3DQ male = 6, hM3DQ female = 7	$F_{\text{virus}}(1,21) = 0.0004, p = 0.98$ $F_{\text{sex}}(1,21) = 0.85, p = 0.37$ $F_{\text{virus} \times \text{sex}}(1,21) = 1.005, p = 0.3276$
Extended Data 3-1A	Relative <i>Oprk1</i> expression, whole brain	Unpaired <i>t</i> test, two-tailed	WT female = 5 <i>Cre</i> /+ female = 5	$t = 7.43, df = 8, p < 0.0001$
Extended Data 3-1B	Relative <i>Oprk1</i> expression, NAc	Unpaired <i>t</i> test, two-tailed	WT male = 4 WT female = 2 <i>Cre</i> /+ male 3 = <i>Cre</i> /+ female = 5	$t = 2.934, df = 12, p = 0.013$
Extended Data 3-2A	Maximal G-protein stimulation	Unpaired <i>t</i> test, two-tailed	WT male = 7 <i>Cre</i> /+ male = 7	$t = 0.12, df = 12, p = 0.9$
Extended Data 3-2B	EC ₅₀	Unpaired <i>t</i> test, two-tailed	WT male = 7 <i>Cre</i> /+ male = 7	$t = 0.07, df = 12, p = 0.95$
Extended Data 3-2C	Basal [³⁵ S]GTP γ S binding	Unpaired <i>t</i> test, two-tailed	WT male = 7 <i>Cre</i> /+ male = 7	$t = 0.22, df = 12, p = 0.83$
Extended Data 3-3A	Amygdala p-ERK/T-ERK	Unpaired <i>t</i> test, two-tailed	WT female = 5, <i>Cre</i> /+ male = 2 male, <i>Cre</i> /+ female = 2	$t = 0.712, df = 7, p = 0.499$
Extended Data 3-3B	Amygdala p-JNK/T-JNK	Unpaired <i>t</i> test, two-tailed	WT female = 5, <i>Cre</i> /+ male = 2 male, <i>Cre</i> /+ female = 2	$t = 0.715, df = 7, p = 0.498$
Extended Data 3-3C	Amygdala P-p38/T-p38	Unpaired <i>t</i> test, two-tailed	WT female = 5, <i>Cre</i> /+ male = 2 male, <i>Cre</i> /+ female = 2	$t = 1.922, df = 6, p = 0.1030$
Extended Data 4-1	Number of closed arm entries, WT vs <i>Oprk1-Cre</i>	Two-way ANOVA	mCherry male = 7, mCherry female = 12; hM3DQ male = 8, hM3DQ female = 7	$F_{\text{genotype}}(1,30) = 1.335, p = 0.26$ $F_{\text{sex}}(1,30) = 0.76, p = 0.39$ $F_{\text{genotype} \times \text{sex}}(1,30) = 0.66, p = 0.43$
Extended Data 7-1	Number of closed arm entries, mCherry vs hM3DQ	Two-way ANOVA	mCherry male = 8, mCherry female = 10; hM3DQ male = 8, hM3DQ female = 9	$F_{\text{virus}}(1,31) = 0.02, p = 0.88$ $F_{\text{sex}}(1,31) = 0.43, p = 0.52$ $F_{\text{virus} \times \text{sex}}(1,31) = 0.62, p = 0.43$
Extended Data 8-1	Difference score percentage (Post-Pre)	Unpaired <i>t</i> test	WT male = 8–10	$t = 2.322, df = 18, p = 0.032$

P, Phosphorylated; T, total.

AP firing (current injection, 0 pA; for 3 min, sampled at 20 kHz) were also collected in current-clamp mode. All recordings were filtered and digitized at 10 kHz. Cells were allowed to equilibrate for 3–5 min before the onset of recordings and each cell was recorded from twice, once at baseline, and 10 min after the addition of 1 μ M CNO (Hello Bio). All protocols were made and run using Clampex (version 11.2) and analyzed using Clampfit (version 10.7.0.3) software (Molecular Devices).

Statistical analyses

All data are presented as the mean \pm SEM. Statistical analysis was assessed using unpaired or paired *t* tests and two-way ANOVA. *Post hoc* Sidak tests were performed when a significant interaction was detected. Curve fit analyses were performed to analyze [³⁵S]GTP γ S binding data. Detailed statistical methods for each figure are provided in an attached table of statistics (Table 1).

Results

We used a variety of techniques to determine whether *Cre* expression was localized exclusively to

Oprk1 cells in the *Oprk1-Cre* mouse. We examined colocalization between *Cre* recombinase and *Oprk1* mRNA in the following three brain regions that express high amounts of *Oprk1*: BLA, claustrum/dorsal endopiriform nucleus, and the PVT. We found a high degree of colocalization between *Oprk1* and *Cre* transcripts in all of the brain regions examined in homozygous *Oprk1-Cre* mice. In the BLA (Fig. 1A), we found that 89% of *Oprk1* transcripts were colocalized with *Cre*. Similarly, we found 95% colocalization in the claustrum/dorsal endopiriform nucleus (Fig. 1B) and ~91.1% colocalization in the PVT (Fig. 1C). These results indicate a high degree of fidelity of *Cre* expression to *Oprk1* cells in these brain regions.

To get a snapshot of *Cre* protein expression in the adult brain, we performed *Cre* IHC in adult homozygous *Oprk1-Cre* mice using a previously validated (Kellendonk et al., 1999) antibody against *Cre* recombinase. We found the highest *Cre*-like immunoreactivity in the claustrum and dorsal endopiriform cortex area. We also found *Cre*-immunoreactive cells in the dorsal and ventral striatum, the CeA, BLA, PVT, VTA, dorsal raphe (DR), and the locus coeruleus (Fig. 2). The pattern of *Cre*-like immunoreactivity closely

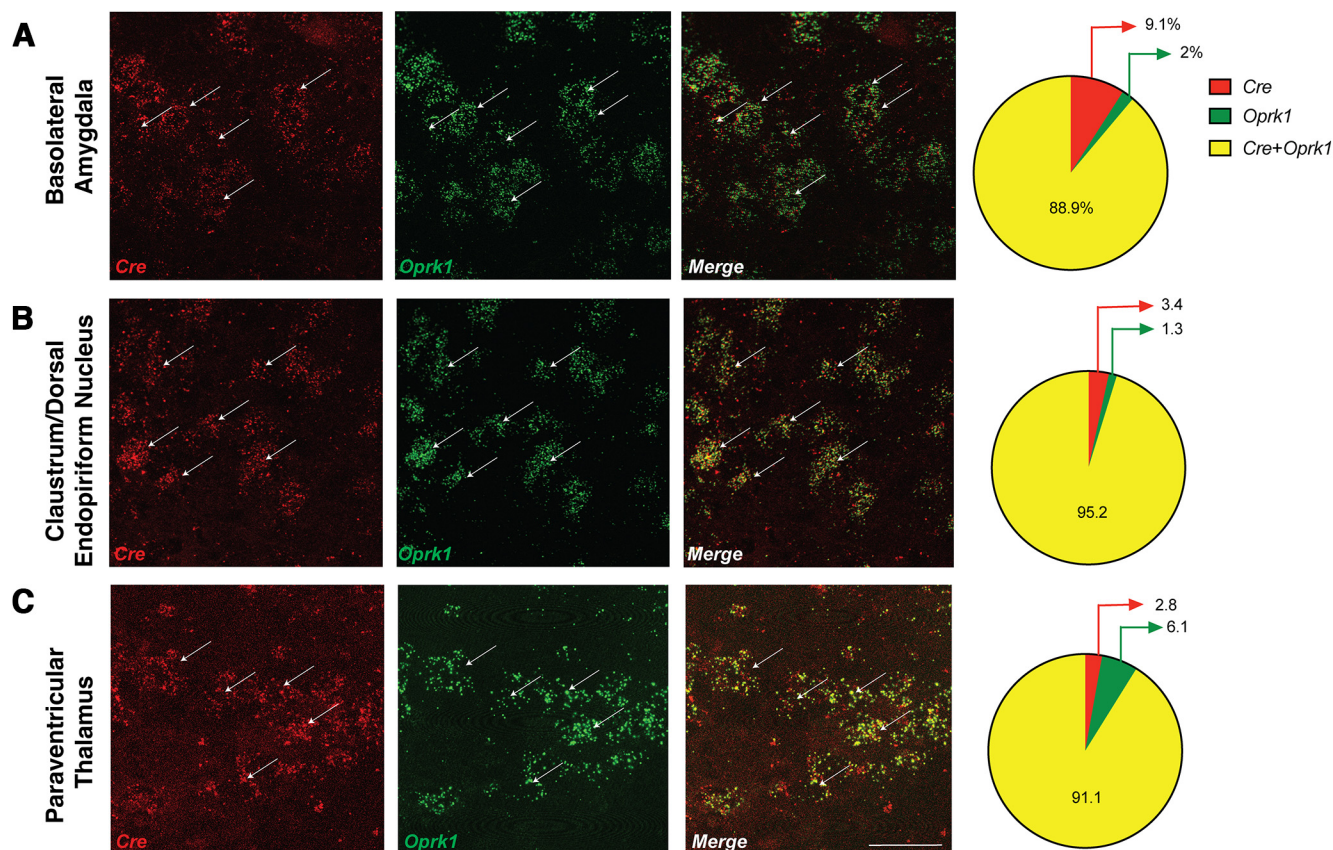


Figure 1. Colocalization of *Oprk1* and *Cre*. **A–C**, *In situ* hybridization using probes targeting *Cre* recombinase and mouse *Oprk1* reveal 80–90% colocalization between *Oprk1* and *Cre* transcripts across the following three brain regions: the BLA (**A**), claustrum/dorsal endopiriform nucleus (**B**), and PVT (**C**). $N = 2$ male mice; $N = 1$ female mouse. Scale bar, 50 μm . See Extended Data Figure 1-1 for generation of *Oprk1-Cre* transgenic mouse.

mimicked the expression pattern of *Oprk1* mRNA in the Allen Brain Atlas.

We also crossed *Oprk1-Cre* mice with the floxed L10A-EGFP reporter mouse (Krashes et al., 2014) to determine the distribution of KOR cells within the BLA. In this mouse, EGFP is expressed in cells that express *Cre* recombinase during development and in adulthood. We found an interesting pattern of *Cre* expression in the BLA of these mice. In the anterior subdivisions of the BLA, EGFP expression, which reports *Cre* expression, was distributed uniformly throughout the BLA. Expression shifted to medial and ventral aspects of the BLA in more posterior subdivisions. This pattern of *Cre* expression closely mirrored the *Oprk1* expression found in the Allen Brain Atlas (Extended Data Fig. 2-1).

We also determined colocalization between virally delivered *Cre*-dependent EGFP and *Oprk1* mRNA expression in the BLA using *in situ* hybridization. Our results revealed that 93% of EGFP-expressing cells also expressed *Oprk1* (Extended Data Fig. 2-2). These results indicate high specificity of viral-mediated labeling of *Oprk1* cells in the BLA.

To determine whether the insertion of *Cre* recombinase into the 3'UTR of the *Oprk1* locus altered *Oprk1* expression, we performed qPCR on whole brain and NAc mRNA from WT and heterozygous *Oprk1-Cre* mice (henceforth

referred to as *Oprk1-Cre* mice). We found an ~0.6-fold increase in *Oprk1* mRNA expression in *Oprk1-Cre* mice compared with WT mice (Extended Data Fig. 3-1A). We also found a similar increase in *Oprk1* mRNA expression in the NAc (Extended Data Fig. 3-1B).

To determine whether this apparent increase in *Oprk1* mRNA levels translates to changes in KOR function, we examined Dyn-induced [^{35}S]GTP- γS binding in striatal membranes prepared from WT and *Oprk1-Cre* mice (Bohn et al., 2015; Zhou et al., 2015; Massaly et al., 2019). Dyn-stimulated GTP- γS binding was similar in both genotypes (Fig. 3A). Basal, E_{max} , and EC_{50} values for [^{35}S]GTP- γS binding (fmole/ μg protein) also did not differ between genotypes (Extended Data Fig. 3-2A–C). Therefore, KOR-G-protein coupling was not altered in *Oprk1-Cre* mice.

We also examined downstream components of KOR signaling in the NAc (Fig. 3B–D) and amygdala (Extended Data Fig. 3-3A–C) of *Oprk1-Cre* mice. KOR activation increases phosphorylation of ERK, JNK, and P38 kinases (Bruchas et al., 2006; Al-Hasani and Bruchas, 2011). We reasoned that if the observed change in *Oprk1* mRNA expression led to a functional change in KOR signaling, we would see an increase in phosphorylation of these downstream effectors. We found no differences in basal phosphorylation levels of ERK, JNK, and P38

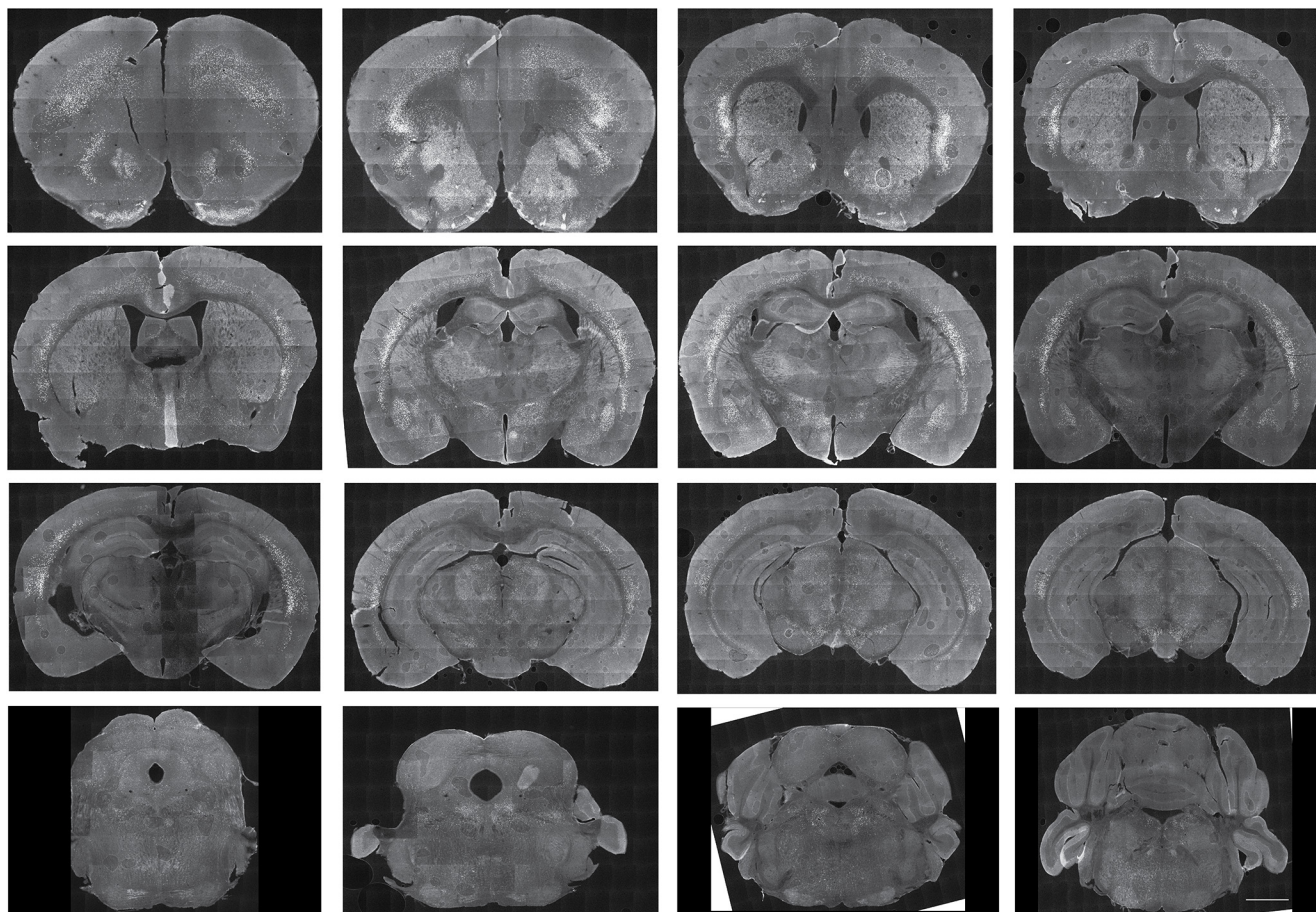


Figure 2. Brain-wide snapshots of Cre expression in the adult *Oprk1-Cre* mouse. Tiled images of Cre protein expression at 20 \times resolution across the brain of an adult *Oprk1-Cre* mouse are shown. Strongest Cre expression was observed in the claustrum and dorsal endopiriform nucleus. Cre expression was also observed in the PVT, CeA, BLA, PVT, DR, and locus coeruleus (LC). The pattern of Cre expression matched that of *Oprk1* expression in the Allen Brain Atlas. Scale bar, 1 mm. Please see Extended Data Figure 2-1 for distribution of BLA^{KOR} cells and Extended Data Figure 2-2 for colocalization between virally delivered Cre-dependent EGFP and *Oprk1* in the BLA.

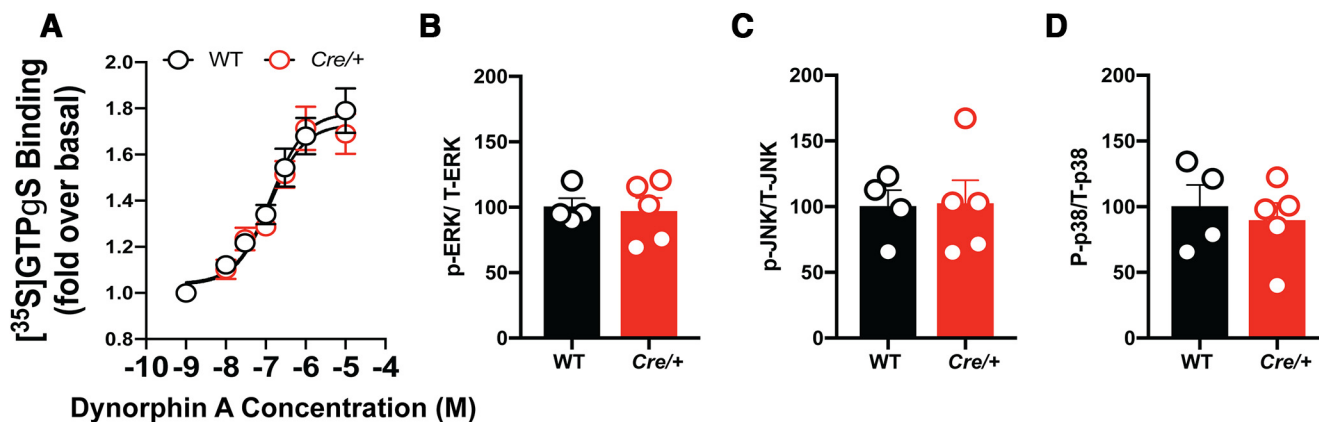


Figure 3. KOR function is intact in *Oprk1-Cre* mice. **A**, Dyn-stimulated GTP γ S binding did not differ significantly between WT and *Oprk1-Cre* mice. $n = 7$ males/group. **B–D**, No differences were observed in phosphorylated (P)-ERK (**B**), P-JNK (**C**), and P-p38 (**D**) in the NAc under basal conditions. $N = 4$ –5/group (WT = 4 females, Cre/+ = 3 females and 2 males). Please see Extended Data Figure 3-1 for *Oprk1* mRNA expression in WT and *Oprk1-Cre* mice; Extended Data Figure 3-2 for [³⁵S]GTP γ S binding in the striatum of WT and *Oprk1-Cre* mice; and Extended Data Figure 3-3 for basal KOR signaling is not altered in the amygdala of *Oprk1-Cre* mice. Extended Data Table 3-1 lists antibodies used for Western blotting.

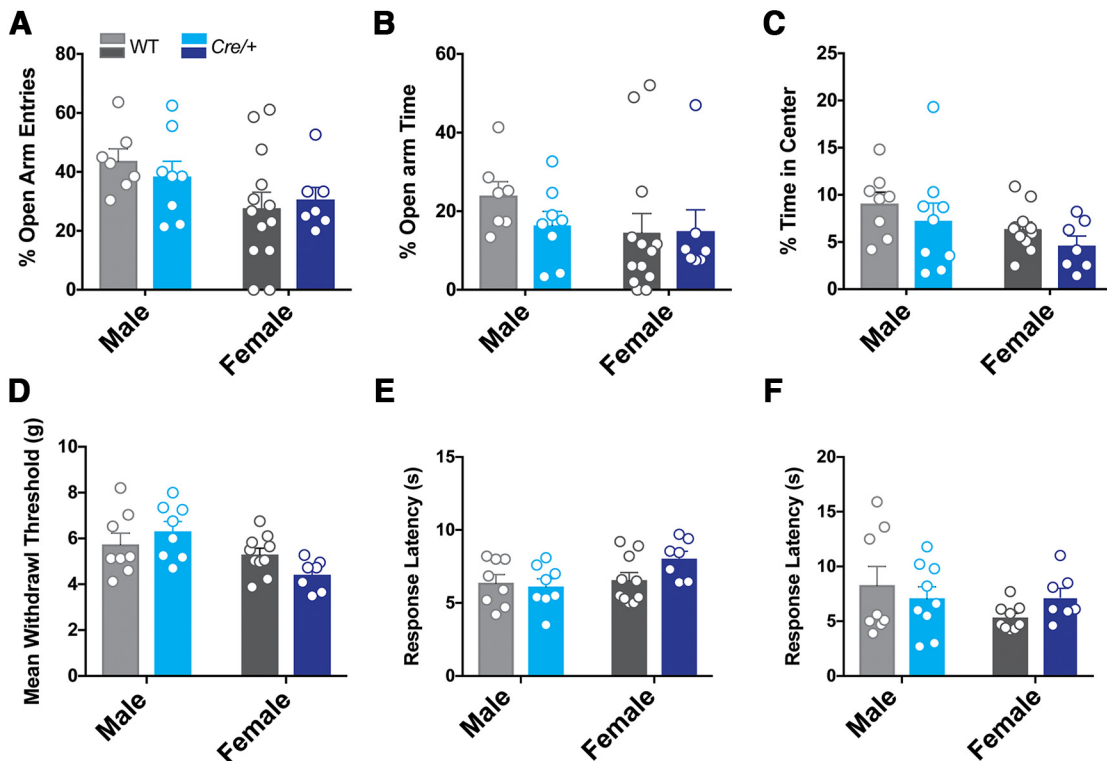


Figure 4. Baseline anxiety-like and pain behaviors in *Oprk1-Cre* mice. **A–C**, Anxiety-like behaviors were tested using the EPM and open field anxiety tests in WT and *Oprk1-Cre* mice. There were no significant genotypic differences in open arm entries (**A**) or time (**B**) in the EPM (WT male = 7, WT female = 12; *Cre/+* male = 8, *Cre/+* female = 7). **C**, There were also no genotypic differences in the percentage of time in the center of the open field (WT male = 8, WT female = 11; *Cre/+* male = 9, *Cre/+* female = 7). **D**, There were no genotype differences seen in the mean withdrawal threshold in the eVF mechanical nociception test (WT male = 8, WT female = 10; *Cre/+* male = 8, *Cre/+* female = 7) and response latencies (**D**) on the hot plate tests (**E**; WT male = 8, WT female = 10; *Cre/+* male = 8, *Cre/+* female = 7) and cold plate tests (**F**) and (WT male = 8, WT female = 9; *Cre/+* male = 9, *Cre/+* female = 7). See Extended Data Figure 4-1 for closed arm entries were not altered on the EPM in *Oprk1-Cre* mice.

kinases in the NAc (Fig. 3B–D) or amygdala (Extended Data Fig. 3-3A–C) between *Oprk1-Cre* mice and their WT littermates, suggesting that the increase in *Oprk1* mRNA did not lead to a functional increase in KOR signaling at baseline.

We next examined whether there were baseline differences in behaviors that are known to be modulated by KOR signaling. First, we examined anxiety-like behaviors using EPM and open field tests. For the EPM, we measured the percentage of open arm entries and the percentage of open arm time (Fig. 4A,B). Two-way ANOVA of the percentage of open arm entries showed a main effect of sex ($F_{\text{sex}(1,30)} = 12.08$, $p = 0.0493$) with females venturing less into the open arms than their male counterparts. However, there was no genotype or genotype \times sex interaction (Fig. 4A). Analysis of the percentage of open arm time did not reveal a main effect of sex, genotype, or genotype \times sex interaction (Fig. 4B). Analysis of the number of closed arm entries also did not reveal main effects of sex, genotype, or sex \times genotype interaction (Extended Data Fig. 4-1). We next examined the percentage of time spent in the center of an open field (Fig. 4C). Two-way ANOVA revealed a main effect of sex ($F_{\text{sex}(1,31)} = 4.4$, $p = 0.04$) with females spending less time exploring the center of the open field. However, we did not detect the main

effects of genotype or genotype \times sex interaction. Next, we examined nociceptive sensitivity in these mice. Since the activation of KORs has analgesic effects (Snyder et al., 2018), we compared nociceptive thresholds between WT and *Oprk1-Cre* mice under basal conditions. We used the electronic von Frey test to measure mechanical nociception and hot and cold plate tests to measure thermal nociception. Two-way ANOVA of mean withdrawal pressure in the eVF test revealed a main effect of sex ($F_{\text{sex}(1,21)} = 9.82$, $p = 0.004$), with females displaying lower mean withdrawal thresholds than males (Fig. 5D). However, there were no main effects of genotype or genotype \times sex interaction. Two-way ANOVA of mean withdrawal latencies on the hot plate and cold plate tests did not reveal significant main effects of sex, genotype, or genotype \times sex interaction (Fig. 4E,F). In summary, we did not detect genotypic differences in any of the baseline behaviors tested.

Since optogenetic stimulation of BLA inputs to the BNST is anxiolytic (Crowley et al., 2016), we predicted that chemogenetic activation of BLA^{KOR} cells would reduce anxiety-like behaviors. We validated DREADD-induced activation of BLA^{KOR} neurons by electrophysiology using amygdala brain slices from *Oprk1-Cre* mice expressing hM3DQ. We found that bath application of CNO (1 μM) significantly increased both spontaneous and

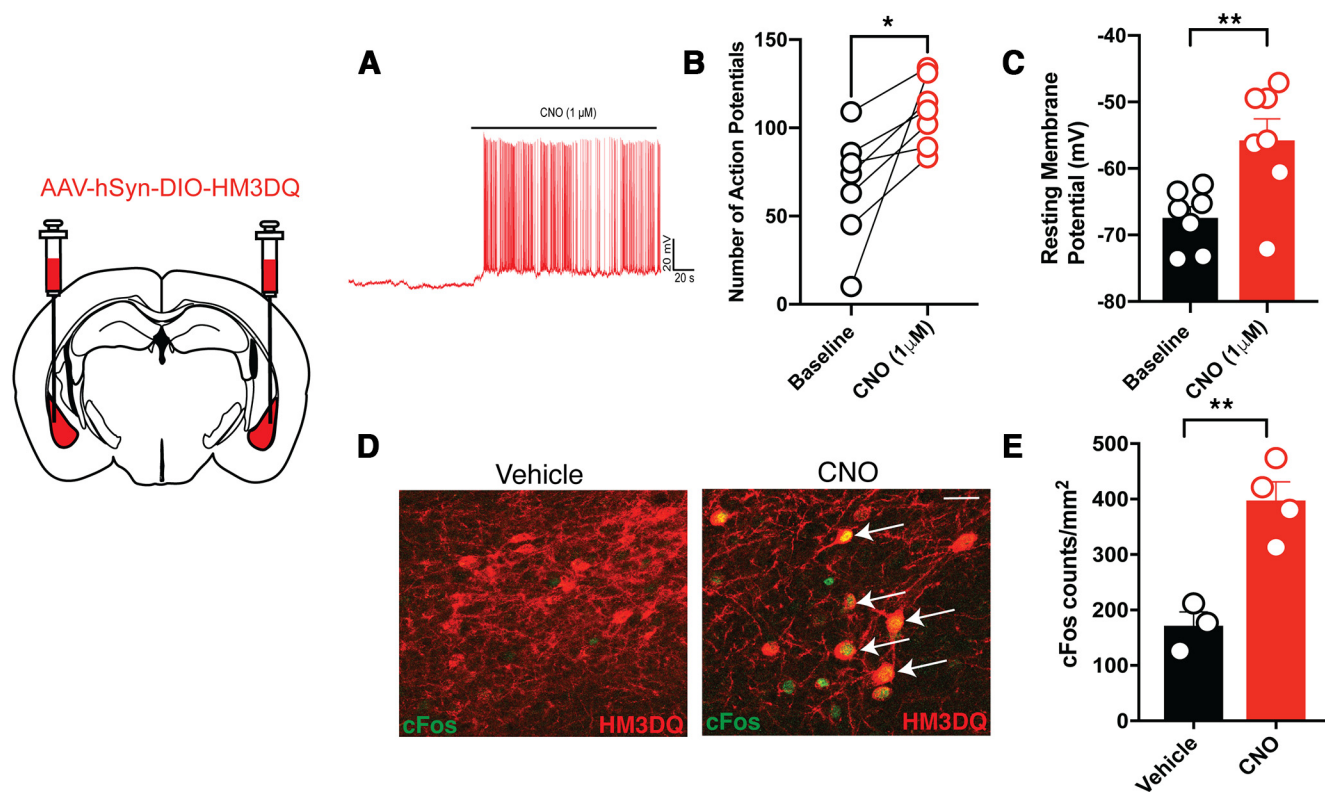


Figure 5. Validation of DREADD-induced activation of BLA^{KOR} neurons. **A–C**, CNO application increased both spontaneous and electrically evoked excitability in BLA^{KOR} cells expressing hM3DQ. * $p = 0.0217$, ** $p = 0.0091$, paired t test, $n = 7$ cells/group. **D**, Visual representation of c-Fos activation in the BLA of hM3DQ-injected *Oprk1-Cre* mice treated with vehicle or CNO before killing. **E**, Quantification of c-Fos shows a significant increase in the activation in CNO-injected mice compared with vehicle-injected mice. ** $p = 0.0041$, unpaired t test, $N = 3–4$ mice/group.

evoked firing of BLA^{KOR} cells expressing hM3DQ (Fig. 5B–D). We also found that intraperitoneal administration of 3 mg/kg CNO significantly increased c-Fos expression in the BLA of hM3DQ-expressing mice compared with mice administered vehicle as a control (Fig. 5E).

We also examined projection targets of BLA^{KOR} cells. We injected Cre-dependent mCherry into the BLA of *Oprk1-Cre* mice and examined mCherry fluorescence throughout the brain. We found strong projections from BLA^{KOR} cells to the mPFC, lateral subdivision of the NAC, claustrum/dorsal endopiriform cortex, and the ventral hippocampus (Fig. 6).

To determine whether the activation of BLA^{KORs} affects anxiety-like behaviors, mice were administered CNO (3 mg/kg) 30 min before the EPM and open field tests. Mice were first tested on the EPM. Two-way ANOVA of the percentage of open arm entries revealed a significant virus \times sex interaction ($F_{\text{virus} \times \text{sex}}(1,31) = 7.491$, $p = 0.0102$). *Post hoc* Sidak test revealed that hM3DQ-injected females made significantly more open arm entries than mCherry controls ($p = 0.0162$; Fig. 7A). Two-way ANOVA of the percentage of time spent in open arms also revealed a significant virus \times sex interaction $F_{\text{virus} \times \text{sex}}(1,31) = 12.22$, $p = 0.0014$. The hM3DQ-injected females spent significantly more time in the open arms than mCherry controls ($p = 0.0010$; Fig. 6B). There were no significant differences in the percentage of open arm entries or the percentage of

open arm time between mCherry and hM3DQ-injected males (Fig. 7A,B). These results indicate an anxiolytic phenotype in hM3DQ-expressing female mice. There were no significant differences in the number of closed arm entries among any of the groups tested (Extended Data Fig. 7-1). Mice were also tested for anxiety-like behaviors on the open field 24 h after the EPM test. Two-way ANOVA of the percentage of time spent in the center of the open field did not reveal any significant main effects of virus, sex, or an interaction between the two (Fig. 7C). No differences were observed between the groups in total distance traveled in the open field (data not shown), suggesting that locomotor activity was not impaired by CNO injections. We next tested the effects of BLA^{KOR} activation on sociability using the three-chamber social interaction test. Two-way ANOVA of the sociability index revealed a significant virus \times sex interaction ($F_{\text{genotype} \times \text{sex}}(1,35) = 6.764$, $p = 0.0135$; Fig. 7D). *Post hoc* analyses did not reveal any significant differences between mCherry-injected and hM3DQ-injected male mice. Female hM3DQ-injected mice displayed increased sociability compared with mCherry controls; however, this result did not reach statistical significance ($p = 0.088$).

KOR agonists are aversive presumably because of KOR-mediated inhibition of target cells (Tejeda and Bonci, 2019). To determine whether BLA^{KORs} contribute to this effect, we sought to counteract KOR inhibition by chemogenetically

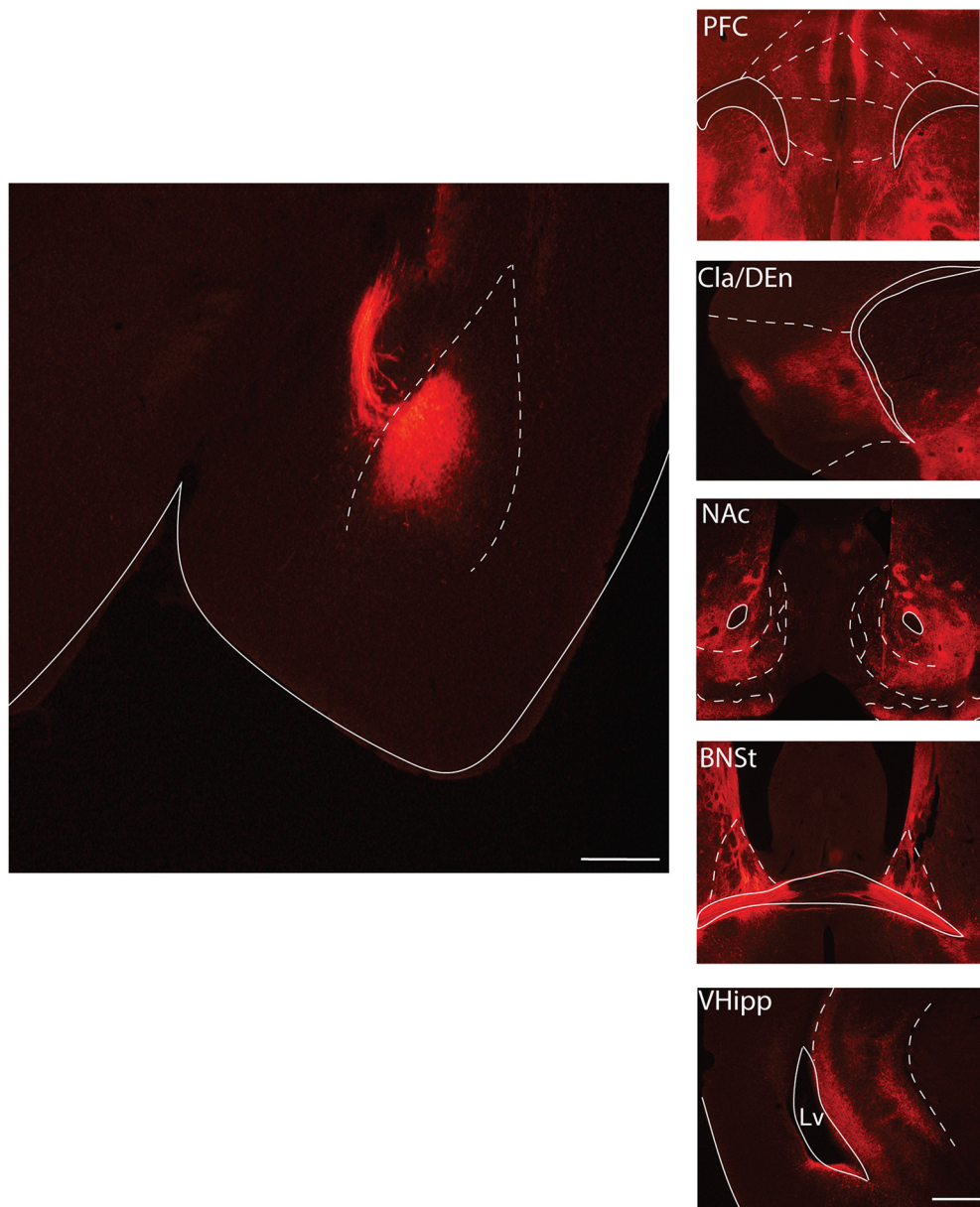


Figure 6. Projections of BLA^{KOR} neurons. Image of mCherry injection into the BLA (left). BLA^{KOR} neurons project to the prefrontal cortex (PFC), the claustrum/dorsal endopiriform nucleus, the NAc, the bed nucleus of the stria terminalis (BNSt), and the ventral hippocampus (VHipp; right).

activating BLA^{KOR} cells. Mice expressing hM3DQ or mCherry were administered vehicle injections and were then confined to one side of the conditioned place preference (CPP) apparatus. Later the same day they received the injections of KOR agonist U-50488 (2.5 mg/kg) and CNO (5 mg/kg) and were confined to the other side. Preference for the drug-paired side before and after conditioning was determined and a difference score was calculated. Two-way ANOVA analysis of the difference scores revealed a significant virus \times sex interaction ($F_{\text{virus} \times \text{sex}}(1,34) = 4.671, p = 0.0378$). Injections of U-50488 plus vehicle produced CPA in mCherry-injected male, but not female, *Oprk1-Cre* mice. CPA was attenuated in U-50488 plus CNO-injected males that expressed

hM3DQ; however, this result did not reach statistical significance ($p = 0.0524$; Fig. 8A). In contrast to males, female mice expressing mCherry or hM3DQ failed to develop CPA (Fig. 8B). Since the magnitude of CPA observed in mCherry-injected *Oprk1-Cre* males is lower ($\sim 15\%$) than what has been reported in the literature (Land et al., 2009), we decided to examine U-50488-induced CPA in C57BL/6J (WT) mice (Extended Data Fig. 8-1). We compared WT mice that received saline injections on both sides of the apparatus to those that received saline on one side and U-50488 (2.5 mg/kg) on the other side. We found that mice that received U-50488 injections showed significant CPA to the drug-paired side compared with mice that received saline on both sides of the chamber (** $p < 0.05$, unpaired t test).

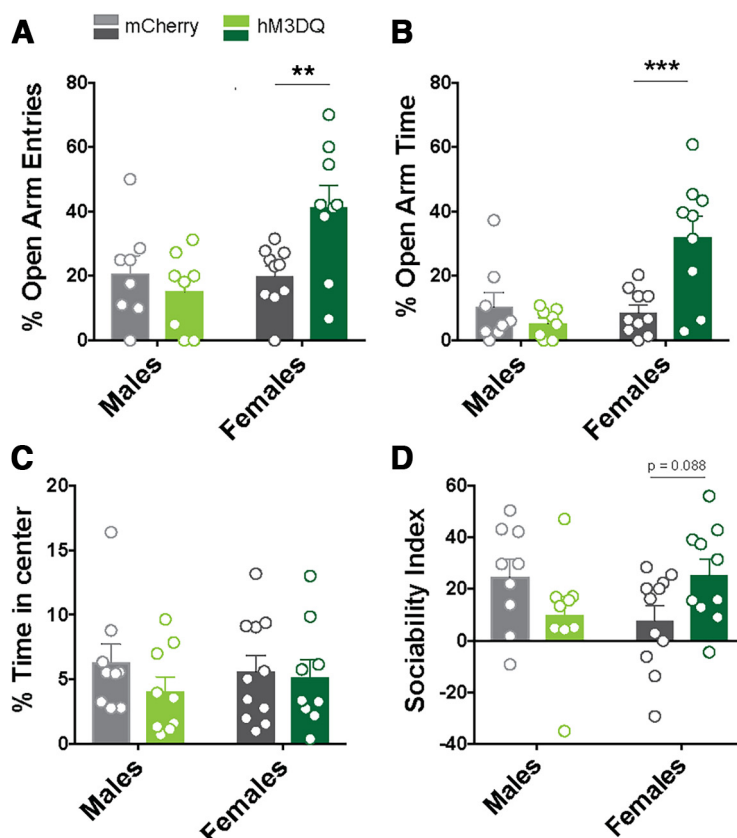


Figure 7. Chemogenetic activation of BLA^{KOR} cells and anxiety-like behavior. **A**, There was no significant difference between mCherry and hM3DQ-injected male mice in open arm entries or open arm time in males ($N = 8/\text{group}$). **B**, There was a significant increase in the percentage of open arm entries (** $p = 0.0016$) and open arm time (*** $p = 0.0010$, Sidak post-test) in hM3DQ-injected female mice compared with mCherry controls ($N = 9\text{--}10$ mice/group). Please see Extended Data Figure 7-1 for closed arm entries in mCherry-injected and hM3DQ-injected mice. **C**, There were no differences in the time spent in the center of an open field in male or female hM3DQ-injected mice compared with mCherry controls (mCherry male = 9, mCherry female = 11; hM3DQ male = 9, hM3DQ female = 9). **D**, There was no difference in sociability index in male mCherry-injected and hM3DQ-injected mice. Female hM3DQ mice showed increased sociability compared with mCherry controls. This result did not reach statistical significance ($p = 0.088$, Sidak post-test; mCherry male = 9, mCherry female = 11; hM3DQ male = 9, hM3DQ female = 10).

Importantly, the magnitude of this CPA (~12%) was similar to that observed in mCherry-injected *Oprk1-Cre* mice.

We next determined whether the activation of BLA^{KOR} cells was inherently reinforcing by measuring the development of CPP after the administration of CNO (5 mg/kg). We observed no significant differences in the percentage of time spent in the CNO-paired compartment before and after conditioning (Fig. 8C,D). Our results indicate that chemogenetic activation of BLA^{KOR} cells by itself is neither aversive nor rewarding. Together, these results suggest that KOR-mediated inhibition of BLA^{KOR} cells contributes to the aversive effects of KOR agonists in males, but not in females.

Discussion

Here we describe the generation and characterization of a transgenic mouse line that expresses Cre recombinase under the control of the *Oprk1* promoter. This mouse was generated to provide a tool for the visualization and manipulation of KOR-expressing neurons throughout the

brain and periphery. Using a variety of methods including IHC, *in situ* hybridization, and virally delivered reporter gene expression, we have shown that Cre recombinase expression in this mouse line is restricted to KOR-expressing cells throughout the brain and that KOR function is preserved in *Oprk1-Cre* mice. We also show functional validation of this mouse line by demonstrating that chemogenetic activation of BLA^{KOR} neurons can modulate anxiety-like behaviors, KOR agonist-induced conditioned aversion, and sociability.

This mouse line differs from the previously published *Oprk1-Cre* line in that the Cre recombinase is inserted into 3'UTR of the KOR locus. In the *Oprk1-Cre* line generated by the Ross laboratory (Cai et al., 2016), the Cre transgene is inserted into the second exon. Therefore, heterozygous Cre mice might be expected to express 50% less KOR than WT littermates. *Oprk1-Cre* mice described in this study show a 0.6-fold increase in *Oprk1* mRNA in several brain regions. We do not know the mechanism for this increase in *Oprk1* mRNA, although one possibility is that insertion of the Cre transgene in the 3'UTR of the

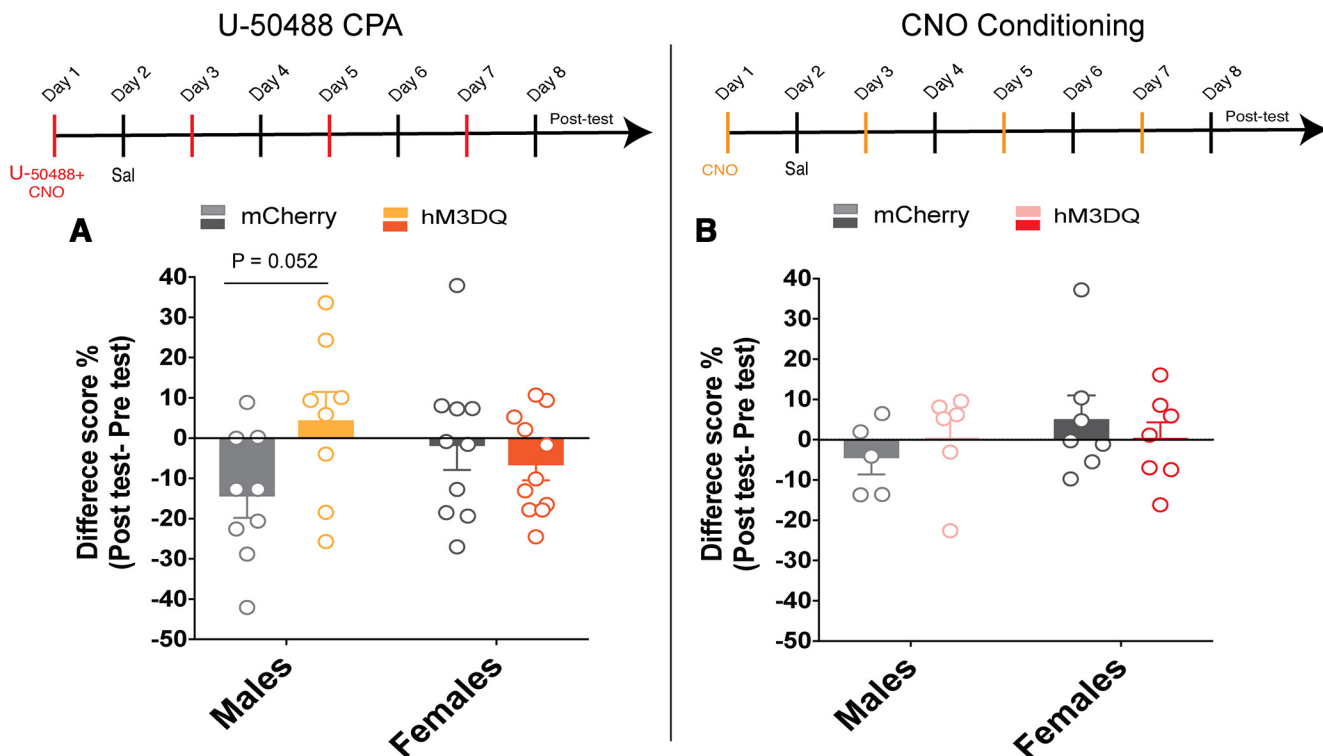


Figure 8. Chemogenetic activation of BLA^{KOR} cells attenuates U-50488 induced CPA. **A**, CNO administration attenuated U-50488-induced CPA in hM3DQ-injected males compared with mCherry controls. However, this effect did not reach statistical significance ($p = 0.0524$, Sidak post-test; $N = 8-9$ /group) in males and in females ($N = 9-11$ /group). **B**, Neither male nor female hM3DQ-injected *Oprk1-Cre* mice form a preference for or avoid the CNO-paired chamber. $N = 5-6$ /group for males and $N = 5-7$ /group for females. See Extended Data Figure 8-1 for U-50488-induced CPA in C57BL/6J mice.

Oprk1 locus may have disrupted an unknown endogenous regulatory element. We investigated whether this change in *Oprk1* mRNA was associated with a functional change in KOR signaling and baseline behaviors known to be sensitive to modulation by KORs. Despite higher levels of mRNA expression, we found no differences in Dyn-stimulated GTP γ S binding in striatal membranes prepared from control and *Oprk1-Cre* mice. We also examined signaling events occurring downstream of KORs including the activation of ERK, JNK, and p38 (Bruchas et al., 2006; Al-Hasani and Bruchas, 2011). We found no differences in the phosphorylation status of key downstream effectors of KOR signaling in the amygdala (CeA plus BLA) and NAc of *Oprk1-Cre* mice compared with WT mice under basal conditions. One caveat with the interpretation of these results is that changes in KOR signaling may be masked under basal conditions and should be examined after KOR agonist treatment to confirm that downstream signaling pathways remain intact in these mice. We also found no differences in baseline nociceptive thresholds and anxiety-like behaviors. Together, these results suggest that the increase in *Oprk1* mRNA did not lead to increased KOR function. We observed this change in *Oprk1* expression despite using a smaller P2A self-cleaving sequence instead of IRES between the KOR coding region and Cre. Changes in expression of an endogenous gene have been reported for other Cre knock-in lines where the Cre transgene has been inserted into the 3'UTR. For

example, the DAT-Flo (Kramer et al., 2021) and the DAT-IRES-Cre lines (Bäckman et al., 2006), in which Cre and Flo transgenes are inserted into the 3' UTR of the DAT locus, both show decreases in DAT expression. Because there are no good commercially available antibodies specific for KOR, the expression of KOR proteins was not directly determined in our mouse line. Regardless, our data reveal that KOR function is unaltered, suggesting that this *Oprk1-Cre* line could be used for a variety of experiments designed to probe the function and anatomy of KOR cells in the brain.

Using RNA *in situ* hybridization, we have shown that Cre expression is localized to *Oprk1*-expressing cells in the following four brain regions: the BLA, claustrum and dorsal endopiriform cortex, and the PVT. We also found that the pattern of Cre protein expression in *Oprk1-Cre* mice closely resembled endogenous *Oprk1* mRNA expression in the brain. Further, we found a high degree of colocalization between virally delivered Cre-dependent EGFP and endogenous *Oprk1* expression in the BLA of *Oprk1-Cre* mice. Based on these results, we conclude that Cre is expressed with high fidelity in KOR-expressing cells. However, researchers interested in using this mouse line will need to confirm this with their chosen Cre-dependent virus or viruses in their brain region of interest.

To demonstrate the utility of these mice in exploring causal relationships between specific KOR cell populations in the brain and behavior, we decided to target KOR-expressing cells in the BLA. We first functionally validated

DREADD expression in the BLA by examining neuronal firing of hM3DQ-expressing cells. We found that CNO application significantly enhanced the firing rate of BLA^{KOR} cells expressing hM3DQ. CNO application also increased c-Fos expression in hM3DQ-expressing BLA^{KOR} cells. CNO injection also resulted in sex-specific effects on the EPM with females displaying reduced anxiety-like behavior. This result is consistent with previous work showing that optogenetic activation of BLA neurons that project to BNST is anxiolytic (Crowley et al., 2016). By contrast, we did not observe any change in anxiety-like behavior in males. Since BLA^{KOR} cells project to many different brain regions, it is possible that selective activation of BNST-projecting BLA^{KOR} cells would have resulted in an anxiolytic phenotype in males. We also observed a trend toward increased sociability after chemogenetic activation of BLA^{KOR} cells in female, but not in male, *Oprk1-Cre* mice. Sex differences have been reported in the role of the Dyn/KOR system in stress reactivity and KOR agonist-induced aversion (Russell et al., 2014; Becker and Chartoff, 2019). Future studies will determine whether these sex differences emerge from changes in receptor density or localization in BLA terminal regions.

We also measured anxiety-like behavior in the open field and failed to observe any significant effects of BLA^{KOR} neuron activation on time spent in the center. One possible reason for this discrepancy with our EPM results could be that the open field is a more anxiogenic environment than the EPM, and indeed control mCherry-injected mice only spent ~5% of their time in the center of the open field. Perhaps, higher doses of CNO are required to induce anxiolysis in such highly anxiogenic environments.

Dyn-mediated activation of KORs has been implicated in the aversive effects of stress. Similarly, pharmacological activation of KORs also results in dysphoria and aversion in rodents as well as in humans (Bruchas et al., 2010; Al-Hasani and Bruchas, 2011; Darcq and Kieffer, 2018). KOR-mediated inhibition of serotonergic neurons in the DRN and dopaminergic neurons in the VTA are implicated in mediating the aversive effects of KOR agonists and stress (Land et al., 2009; Bruchas et al., 2011). However, the contribution of BLA^{KORs} in the aversive effects of KOR activation remain unknown. Our results revealed that U-50488 treatment induced CPA in males but not females and that hM3DQ-mediated activation of BLA^{KOR} cells attenuated U-50488-induced CPA in males. These results implicate a role for KORs expressed in the BLA in regulating KOR agonist-mediated aversion, although we did not include a control group injected with vehicle+U-504888. Further, the magnitude of U-50488-induced CPA was similar in both male *Oprk1-Cre* and WT C57BL/6J mice suggesting intact in vivo KOR agonist efficacy in *Oprk1-Cre* mice. BLA^{KOR} cells project to the mPFC, NAc, ventral hippocampus, and insular cortex. Future studies will determine which of these downstream projection targets of BLA^{KOR} encode this aversion. Surprisingly, we failed to observe U-50488-induced CPA in females. One possible reason for this could be that higher doses of U-50488 are required to produce CPA in females.

We next investigated whether the activation of BLA^{KOR} cells themselves was rewarding. Our CNO place conditioning

results reveal that repeated activation of BLA^{KOR} cells did not produce conditioned place preference or aversion. Optogenetic stimulation of BLA inputs to the NAc is highly rewarding and promotes self-stimulation (Stuber et al., 2011). By contrast, optical activation of BLA cell bodies was highly variable in supporting self-stimulation, suggesting that BLA regulates reward and reinforcement in a projection-specific manner. In summary, these results suggest that the inhibition of BLA^{KOR} cells by KOR agonists may in part underlie the aversive effects of KOR agonists.

In summary, we have generated a transgenic Cre-driver mouse line that expresses Cre recombinase under the control of the KOR promoter. In this mouse, Cre is expressed with very high fidelity in KOR cells. This mouse could be an important tool that allows for mapping the projections of KOR cells and dissecting the contribution of KOR circuits throughout the brain in addiction, pain, and stress-related behaviors.

References

- Abraham AD, Casello SM, Schattauer SS, Wong BA, Mizuno GO, Mahe K, Tian L, Land BB, Chavkin C (2021) Release of endogenous dynorphin opioids in the prefrontal cortex disrupts cognition. *Neuropsychopharmacology* 46:2330–2339.
- Al-Hasani R, Bruchas MR (2011) Molecular mechanisms of opioid receptor-dependent signaling and behavior. *Anesthesiology* 115:1363–1381.
- Bäckman CM, Malik N, Zhang Y, Shan L, Grinberg A, Hoffer BJ, Westphal H, Tomac AC (2006) Characterization of a mouse strain expressing Cre recombinase from the 3' untranslated region of the dopamine transporter locus. *Genesis* 44:383–390.
- Becker JB, Chartoff E (2019) Sex differences in neural mechanisms mediating reward and addiction. *Neuropsychopharmacology* 44:166–183.
- Bohn LM, Zhou L, Ho JH (2015) Approaches to assess functional selectivity in GPCRs: evaluating G protein signaling in an endogenous environment. *Methods Mol Biol* 1335:177–189.
- Bruchas MR, Macey TA, Lowe JD, Chavkin C (2006) Kappa opioid receptor activation of p38 MAPK is GRK3- and arrestin-dependent in neurons and astrocytes. *J Biol Chem* 281:18081–18089.
- Bruchas MR, Land BB, Aita M, Xu M, Barot SK, Li S, Chavkin C (2007a) Stress-induced p38 mitogen-activated protein kinase activation mediates κ -opioid-dependent dysphoria. *J Neurosci* 27:11614–11623.
- Bruchas MR, Yang T, Schreiber S, Defino M, Kwan SC, Li S, Chavkin C (2007b) Long-acting kappa opioid antagonists disrupt receptor signaling and produce noncompetitive effects by activating c-Jun N-terminal kinase. *J Biol Chem* 282:29803–29811.
- Bruchas MR, Land BB, Chavkin C (2010) The dynorphin/kappa opioid system as a modulator of stress-induced and pro-addictive behaviors. *Brain Res* 1314:44–55.
- Bruchas MR, Schindler AG, Shankar H, Messinger DI, Miyatake M, Land BB, Lemos JC, Hagan CE, Neumaier JF, Quintana A, Palmiter RD, Chavkin C (2011) Selective p38 α MAPK deletion in serotonergic neurons produces stress resilience in models of depression and addiction. *Neuron* 71:498–511.
- Cai X, Huang H, Kuzirian MS, Snyder LM, Matsushita M, Lee MC, Ferguson C, Homanics GE, Barth AL, Ross SE (2016) Generation of a KOR-Cre knockin mouse strain to study cells involved in kappa opioid signaling. *Genesis* 54:29–37.
- Chavkin C, Koob GF (2016) Dynorphin, dysphoria, and dependence: the stress of addiction. *Neuropsychopharmacology* 41:373–374.
- Crowley NA, Kash TL (2015) Kappa opioid receptor signaling in the brain: circuitry and implications for treatment. *Prog Neuropsychopharmacol Biol Psychiatry* 62:51–60.

- Crowley NA, Bloodgood DW, Hardaway JA, Kendra AM, McCall JG, Al-Hasani R, McCall NM, Yu W, Schools ZL, Krashes MJ, Lowell BB, Whistler JL, Bruchas MR, Kash TL (2016) Dynorphin controls the gain of an amygdalar anxiety circuit. *Cell Rep* 14:2774–2783.
- Darcq E, Kieffer BL (2018) Opioid receptors: drivers to addiction? *Nat Rev Neurosci* 19:499–514.
- DePaoli AM, Hurley KM, Yasada K, Reisine T, Bell G (1994) Distribution of kappa opioid receptor mRNA in adult mouse brain: an in situ hybridization histochemistry study. *Mol Cell Neurosci* 5:327–335.
- Inan S, Cowan A (2022) Antipruritic effects of kappa opioid receptor agonists: evidence from rodents to humans. *Handb Exp Pharmacol* 271:275–292.
- Kellendonk C, Tronche F, Casanova E, Anlag K, Opherk C, Schütz G (1999) Inducible site-specific recombination in the brain. *J Mol Biol* 285:175–182.
- Kramer DJ, Aisenberg EE, Kosillo P, Friedmann D, Stafford DA, Lee AY, Luo L, Hockemeyer D, Ngai J, Bateup HS (2021) Generation of a DAT-P2A-Flpo mouse line for intersectional genetic targeting of dopamine neuron subpopulations. *Cell Rep* 35:109123.
- Krashes MJ, Shah BP, Madara JC, Olson DP, Strohlic DE, Garfield AS, Vong L, Pei H, Watabe-Uchida M, Uchida N, Liberles SD, Lowell BB (2014) An excitatory paraventricular nucleus to AgRP neuron circuit that drives hunger. *Nature* 507:238–242.
- Krystal AD, Pizzagalli DA, Smoski M, Mathew SJ, Nurnberger J, Lisanby SH, Iosifescu D, Murrrough JW, Yang H, Weiner RD, Calabrese JR, Sanacora G, Hermes G, Keefe RSE, Song A, Goodman W, Szabo ST, Whitton AE, Gao K, Potter WZ (2020) A randomized proof-of-mechanism trial applying the “fast-fail” approach to evaluating κ -opioid antagonism as a treatment for anhedonia. *Nat Med* 26:760–768.
- Land BB, Bruchas MR, Schattauer S, Giardino WJ, Aita M, Messinger D, Hnasko TS, Palmiter RD, Chavkin C (2009) Activation of the kappa opioid receptor in the dorsal raphe nucleus mediates the aversive effects of stress and reinstates drug seeking. *Proc Natl Acad Sci U S A* 106:19168–19173.
- Lasek AW, Azouaou N (2010) Virus-delivered RNA interference in mouse brain to study addiction-related behaviors. *Methods Mol Biol* 602:283–298.
- Maiya R, Pomrenze MB, Tran T, Tiwari GR, Beckham A, Paul MT, Dayne Mayfield R, Messing RO (2021) Differential regulation of alcohol consumption and reward by the transcriptional cofactor LMO4. *Mol Psychiatry* 26:2175–2186.
- Massaly N, Copits BA, Wilson-Poe AR, Hipólito L, Markovic T, Yoon HJ, Liu S, Walicki MC, Bhatti DL, Sirohi S, Klaas A, Walker BM, Neve R, Cahill CM, Shoghi KI, Gereau RW, McCall JG, Al-Hasani R, Bruchas MR, Morón JA (2019) Pain-induced negative affect is mediated via recruitment of the nucleus accumbens kappa opioid system. *Neuron* 102:564–573 e6.
- McDonald J, Lambert DG (2010) Binding of GTPgamma[35S] is regulated by GDP and receptor activation. Studies with the nociceptin/orphanin FQ receptor. *Br J Pharmacol* 159:1286–1293.
- Nemeroff CB, Vale WW (2005) The neurobiology of depression: inroads to treatment and new drug discovery. *J Clin Psychiatry* 66:5–13.
- Nestler EJ (1996) Under siege: the brain on opiates. *Neuron* 16:897–900.
- Nguyen E, Lim G, Ding H, Hachisuka J, Ko MC, Ross SE (2021) Morphine acts on spinal dynorphin neurons to cause itch through disinhibition. *Sci Transl Med* 13:eabc3774.
- Pomrenze MB, Giovanetti SM, Maiya R, Gordon AG, Kreeger LJ, Messing RO (2019) Dissecting the roles of GABA and neuropeptides from rat central amygdala CRF neurons in anxiety and fear learning. *Cell Rep* 29:13–21.e4.
- Russell SE, Rachlin AB, Smith KL, Muschamp J, Berry L, Zhao Z, Chartoff EH (2014) Sex differences in sensitivity to the depressive-like effects of the kappa opioid receptor agonist U-50488 in rats. *Biol Psychiatry* 76:213–222.
- Schindelin J, Arganda-Carreras I, Frise E, Kaynig V, Longair M, Pietzsch T, Preibisch S, Rueden C, Saalfeld S, Schmid B, Tinevez JY, White DJ, Hartenstein V, Eliceiri K, Tomancak P, Cardona A (2012) Fiji: an open-source platform for biological-image analysis. *Nat Methods* 9:676–682.
- Snyder LM, et al. (2018) Kappa opioid receptor distribution and function in primary afferents. *Neuron* 99:1274–1288.e6.
- Stuber GD, Sparta DR, Stamatakis AM, van Leeuwen WA, Hardjoprajitno JE, Cho S, Tye KM, Kempadoo KA, Zhang F, Deisseroth K, Bonci A (2011) Excitatory transmission from the amygdala to nucleus accumbens facilitates reward seeking. *Nature* 475:377–380.
- Tejeda HA, Bonci A (2019) Dynorphin/kappa-opioid receptor control of dopamine dynamics: implications for negative affective states and psychiatric disorders. *Brain Res* 1713:91–101.
- Zhou L, Stahl EL, Lovell KM, Frankowski KJ, Prisinzano TE, Aubé J, Bohn LM (2015) Characterization of kappa opioid receptor mediated, dynorphin-stimulated [35S]GTP γ S binding in mouse striatum for the evaluation of selective KOR ligands in an endogenous setting. *Neuropharmacology* 99:131–141.